Direct Calculation of the HBT Equivalent Circuit From Measured S-Parameters

David R. Pehlke and Dimitris Pavlidis

Center for High Frequency Microelectronics
Solid State Electronics Laboratory
The University of Michigan, Ann Arbor, MI 48109-2122

Abstract

A new approach for directly calculating the HBT equivalent circuit from measured S-parameters is presented. Analytically derived rather then fitted solutions are obtained in this way. Extrinsic as well as intrinsic element values are computed without the use of special test structures or additional measurement steps. Bias dependent results for base resistance, collector resistance, base-collector capacitance, base transport factor, and base and collector transit times are discussed in detail.

I. Introduction

HBTs have recently demonstrated significantly improved RF performance into the mm-wave frequencies with the advent of self-aligned technologies, innovative isolation approaches to reduce parasitic effects, and exploitation of ballistic transport in the base-collector depletion region. As these technologies mature and parasitic resistances and capacitances are minimized, it becomes increasingly important to analyze the exact causes of device limitations in terms of the HBT device physics and equivalent circuit representation. By studying the impact of particular transit times, resistances and capacitances on the device performance, we may then apply technologies to best optimize those aspects that limit the device performance. Fitting routines to numerically optimize relatively large equivalent circuits to match measured data may result in non-unique solutions for element values that depend on starting conditions [1]. Parameter extraction techniques for HBTs have been reported by D.Costa, et al [2] and other groups [3]. However, even the best of those approaches require some separate measurement of test structures to characterize parasitics, whose effect is then mathematically subtracted out before calculating the intrinsic circuit, whereas the approach presented in this paper does not require this. Direct calculation of the HBT equivalent circuit from S-parameter measurements with detailed bias-dependent results of base resistance, collector resistance, base-collector capacitance, frequency dependence of $\alpha(\omega)$, and exact values of base and collector transit times are discussed using the proposed new technique.

This work is being supported by the Army Research Office under the URI program, Contract No. DAAL03-87-K-0007

II. HBT Equivalent Circuit Extraction Formalism

The GaAs/AlGaAs HBTs characterized in this work were fabricated at the University of Michigan using a self-aligned technology allowing 0.1 μm separation between base ohmic metal and active emitter[4]. The HBT equivalent circuit used for this work is the conventionally accepted T-model shown in Figure 1 along with a table of calculated element values using our method. The approach presented in this paper allows the evaluation of the impedances corresponding to the outlined circuit blocks of Figure 1. Information on the individual elements contained in these blocks can be obtained by examining the frequency dependences of the

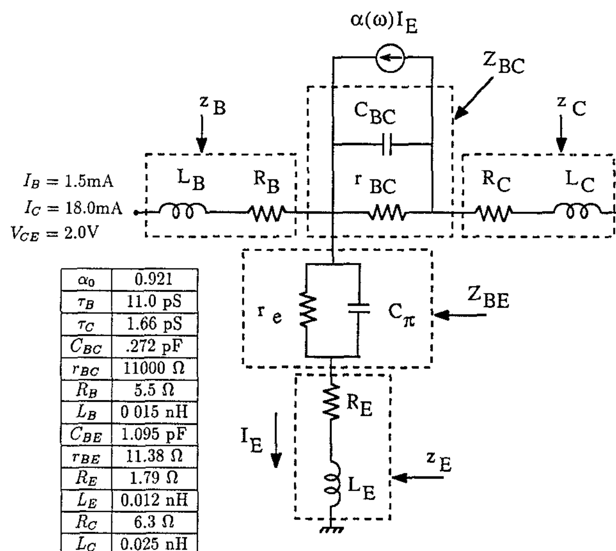

α_0	0.921
τ_B	11.0 pS
τ_C	1.66 pS
C_{BC}	.272 pF
r_{BC}	11000 Ω
R_B	5.5 Ω
L_B	0 015 nH
C_{BE}	1.095 pF
r_{BE}	11.38 Ω
R_E	1.79 Ω
L_E	0.012 nH
R_C	6.3 Ω
L_C	0.025 nH

Figure 1: HBT T-Model Equivalent Circuit and Parameters Extracted Using the Proposed Technique

CH3141-9/92/0000-0735$01.00 © 1992 IEEE

block impedance. The HBT extrinsic H-parameter formulation for the equivalent circuit of Figure 1 is :

$$H_{11} = z_B + \frac{(Z_{BE} + z_E)(Z_{BC} + z_C)}{(Z_{BE} + z_E + z_C) + Z_{BC}(1-\alpha)} \quad (1)$$

$$H_{21} = \frac{\alpha Z_{BC} - (Z_{BE} + z_E)}{(Z_{BE} + z_E + z_C) + Z_{BC}(1-\alpha)} \quad (2)$$

$$H_{12} = \frac{Z_{BE} + z_E}{(Z_{BE} + z_E + z_C) + Z_{BC}(1-\alpha)} \quad (3)$$

$$H_{22} = \frac{1}{(Z_{BE} + z_E + z_C) + Z_{BC}(1-\alpha)} \quad (4)$$

And the solution of the circuit blocks of Figure 1 may then be calculated in terms of the extrinsic H-parameters as:

$$z_B = \frac{H_{11}H_{22} - H_{12}H_{21} - H_{12}}{H_{22}} \quad (5)$$

$$Z_{BC} + z_C = \frac{1 + H_{21}}{H_{22}} \quad (6)$$

$$Z_{BE} + z_E = \frac{H_{12}}{H_{22}} \quad (7)$$

$$\alpha Z_{BC} = \frac{H_{21} + H_{12}}{H_{22}} \quad (8)$$

Measured S-parameters are converted to H-parameters and then the sub-circuits described above are calculated directly. Each of the parameters contained in the circuit blocks are then extracted by studying the frequency dependent characteristics of the blocks as is explained below with illustrated examples.

III. HBT Characteristics Based on the Proposed Formalism

The self-aligned GaAs/AlGaAs HBTs were measured from 0.5 GHz to 26 GHz using a Cascade Microtech on-wafer probe station and hp8510 Network Analyzer. The equivalent circuit parameters of the HBTs are calculated based on the formalism outlined in section II.

A. Base Resistance (R_B) and Inductance (L_B)

From Figure 1, we see that z_B is simply a series R-L circuit with its real part equal to R_B, the base resistance of the HBT. By calculating z_B from equation 5 using the evaluated H_{ij} parameters, we pull out R_B as its real part. Figure 2 shows that the values of base resistance calculated directly from these measurements have a slight bias dependence on injection level, and decreases slightly as the base current injection level is increased. These results provide good physical insight into the fact that the base resistance is made up of three parts :

$$R_B = r_{B\Omega} + r_{BS} + r_B \quad (9)$$

where $r_{B\Omega}$ is the base ohmic metal contact resistance, r_{BS}

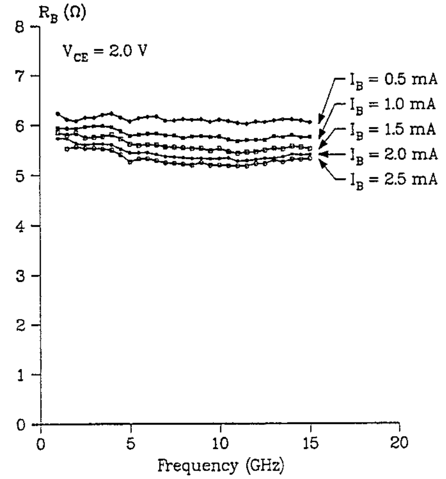

Figure 2: Base Resistance vs. Frequency Showing the Reduction of Base Resistance as the Injection Level is Increased

is the series access component of the base resistance, and r_B is the active device spreading resistance. $r_{B\Omega}$ and r_{BS} are bias independent, while r_B should decrease as the collector current in the HBT is increased, resulting in the trend as seen in Figure 2. The series base inductance, L_B, is found in a similar way realizing that the imaginary part of z_B is simply ωL_B. Both R_B and L_B values are entered in the results for the tested device of Figure 1.

B. Collector Resistance (R_C)

The representation of $Z_{BC} + z_C$ above reveals that its real part is made up of a frequency dependent part involving C_{BC} and r_{BC} along with a constant part made up of R_C. At high frequencies, the real part of $Z_{BC} + z_C$ will decay to this constant value of R_C and the bias dependence of this is shown in Figure 3. We see that the value of R_C arrived at is independent of injection levels as is expected for this series access resistance.

C. Base-Collector Capacitance (C_{BC}) and Collector Inductance (L_C)

The imaginary part of $Z_{BC} + z_C$ is dominated by C_{BC} at low frequencies. This is due to the large isolation resistance, r_{BC}, causing the imaginary part of $Z_{BC} + z_C$ to asymptotically approach $-1/\omega C_{BC}$ as the frequency becomes small. For these devices this applies below approximately 5GHz and C_{BC} can be pulled out directly as seen in Figure 4 as a function of V_{CE}. The C_{BC} value is found to drop in a square root dependence with applied reverse bias across the base-collector junction as is theoretically expected. The results vary less than 1% across this 1GHz-5GHz frequency band. At higher frequencies, both C_{BC} and L_C contribute to the imaginary part of $Z_{BC} + z_C$, and once C_{BC} is determined, L_C can also be directly calculated. (See results of Figure 1).

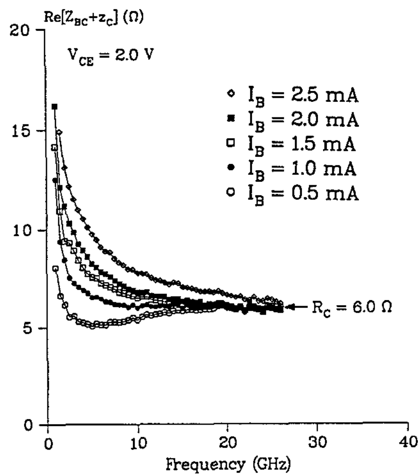

Figure 3: Collector Resistance vs. Frequency Showing the Bias Independent Behavior of the Collector Series Access Resistance

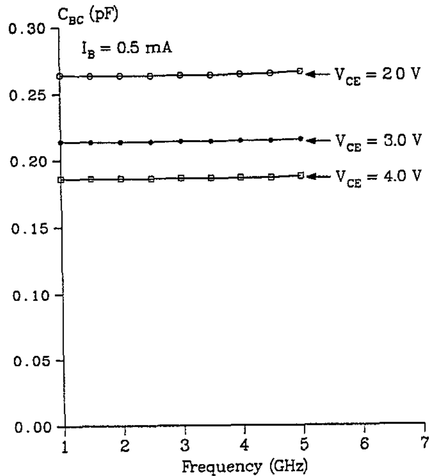

Figure 4: Base-Collector Capacitance vs. Frequency at $I_B = 0.5mA$ Showing the Expected Decrease in C_{BC} as V_{CE} is Increased

D. Base-Collector Isolation Resistance (r_{BC})

At lower frequencies, the impedance due to the base-collector capacitance C_{BC} starts to increase and it becomes a much less efficient feed-through element. We then start to see the effect of the large isolation resistance r_{BC} in parallel with it, and the real part of $Z_{BC} + z_C$ increases dramatically, with the real part of $r_{BC}//C_{BC}$ becoming much larger than the collector series resistance r_C. In order to accurately extract r_{BC}, it is critical to measure device results at frequencies low enough to see the region where r_{BC} dominates this behavior (see results of Figure 1 for the r_{BC} value of the tested device).

E. Base Transport Factor ($\alpha(\omega)$)

The base transport factor, $\alpha(\omega)$, can be calculated once C_{BC} is known by realizing that the imaginary part of Z_{BC} ($\approx -1/\omega C_{BC}$) is much larger than its real part and dominates Z_{BC} in the expression for αZ_{BC}. The previously calculated value for C_{BC} is then used to calculate the real and imaginary parts of α from αZ_{BC}. The result for $|\alpha(\omega)|$ is shown in Figure 5 and the result for $\angle\alpha(\omega)$ is shown in Figure 6. The symbol points are the values directly calculated from the S-parameters using the approach presented in this paper. The solid lines are theoretically calculated curves from the measured data fitting the following expression [5]

$$\alpha(\omega) = \frac{\alpha_0}{1 + \frac{j\omega}{\omega_\beta}} e^{-j\omega(\frac{m\tau_B}{1.2} + \frac{\tau_C}{2})} \qquad (10)$$

where τ_B is the base transit time, τ_C is the collector transit time, $\omega_\beta = 1.2/\tau_B$ is the 3dB frequency of the α expression and m=0.22 is the empirical factor employed to match the phase of the 3dB roll-off approximation for $\alpha(\omega)$ to its more accurate hyperbolic secant representation. As can be seen, the directly calculated values are in excellent agreement with the theoretical model of equation (10). This is to the best of our knowledge the first demonstration of direct calculation from measured S-parameters of the frequency dependence of the intrinsic base transport factor. Traditional techniques have relied on fitting and /or separate measurement for parasitic de-embedding before intrinsic small-signal parameters of this kind are extracted.

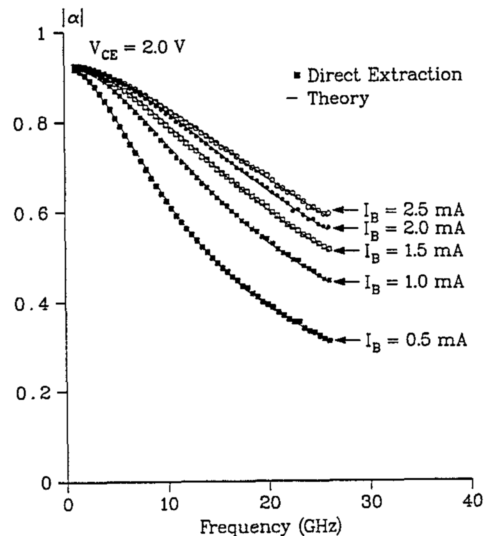

Figure 5: Intrinsic Base Transport Factor Magnitude vs. Frequency Showing Excellent Agreement with Theoretical Expectations as Well as the Gain Improvement with Bias

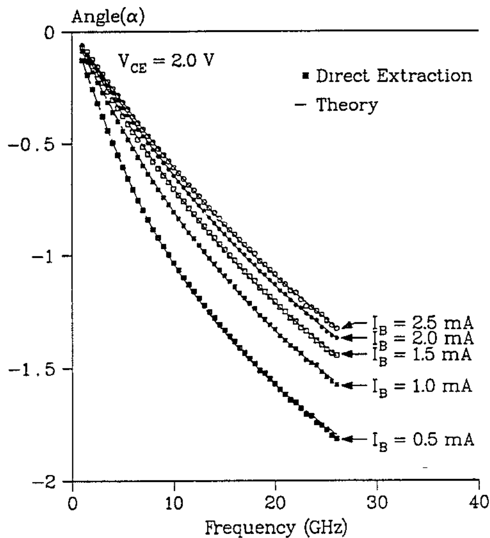

Figure 6: Intrinsic Base Transport Factor Phase Angle vs. Frequency Showing Excellent Agreement with Theoretical Expectations as Well as the Gain Improvement with Bias

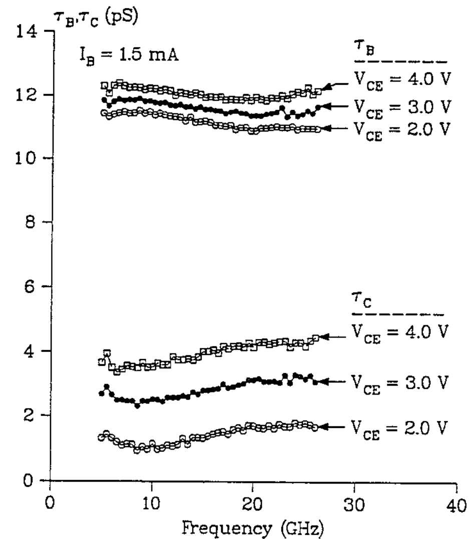

Figure 7: Base and Collector Transit Times vs. Frequency Showing The Increase in Transit Time with V_{CE}

F. Base-Emitter Junction and Emitter Parasitics

Once $\alpha(\omega)$ is found, we can apply the expressions for device input resistance, r_e, and base-emitter capacitance, C_π, found in [5] to the calculated values of $Z_{BE}+z_E$ according to equation (7). Unfortunately, we are unable to calculate any single element exactly because of the number of unknowns in this block of the circuit, but can significantly reduce the error for a fitting routine by fixing the $\alpha(\omega)$ expression extracted above. By doing this we reduce the number of unknowns to just four elements, r_e,C_π,R_E,L_E, and are able to apply optimization to this reduced subcircuit with added confidence.

G. Base and Collector Transit Times (τ_B, τ_C)

The only unknowns in the expression for the magnitude $|\alpha(\omega)|$ shown in Figure 5, are the DC value of the transport factor, α_0, and the alpha $3dB$ frequency, ω_β. By taking α_0 to be the value approached by $|\alpha(\omega)|$ at low frequency, we are left with only one unknown and can calculate ω_β (and therefore the base transit time $\tau_B = 1.2/\omega_\beta$) directly at each frequency. The phase angle of the base transport factor, $\angle\alpha(\omega)$, is shown in Figure 6 and depends only on τ_B and the collector transit time τ_C. With τ_B known at each frequency, we may then use $\angle\alpha(\omega)$ to calculate τ_C at each frequency using equation 10. As is shown in Figure 7, the transit time in these devices is dominated by base diffusion of minority carriers and both base and collector transit times exhibit bias dependencies. The collector transit time increases with increased reverse bias on the base-collector junction as is expected as that depletion region thickness swells.

IV. Conclusions

In summary, we have demonstrated a formalism for direct calculation of the HBT equivalent circuit from measured S-parameters without test structure characterization and a minimum of numerical fitting. This approach can serve as a useful tool toward optimization of process technologies and HBT high-speed performance, revealing the factors that limit device performance and allowing direct insight into the HBT device physics.

References

[1] R.L. Vaitkus. *Uncertainty in the Values of GaAs MESFET Equivalent Circuit Elements Extracted From Two-Port Scattering Parameters.* Proceedings IEEE/Cornell Conference on High-Speed Semiconductor Devices and Circuits, pp. 301-308, 1983.

[2] D. Costa, W.U. Liu and J.S. Harris, *Direct Extraction of the AlGaAs/GaAs Heterojunction Bipolar Transistor Small-Signal Equivalent Circuit* IEEE Transactions on Electron Devices, Vol. 38, pp. 2018-2024, September,1991.

[3] H. Cho and D.E. Burke, *A Simple Model for Distributed Base Impedance with AC Verification Using S-Parameter Measurements* IEEE 1990 Bipolar Circuits and Technology Meeting, 5.3, pp. 106-109.

[4] D. Pehlke and D. Pavlidis, *Critical Issues in Process Technology for High-Speed Self-Aligned GaAs/AlGaAs Heterojunction Bipolar Transistors*, Digest of the GaAs Manufacturing and Technology Conference, Reno, Nevada, pp. 93-96, April, 1991

[5] A.P. Laser and D. Pulfrey, *Reconciliation of Methods for Estimating f_{MAX} for Microwave Heterojunction Transistors*, IEEE Transactions on Electron Devices, Vol. 38, pp. 1685-1692, August,1991.